The effects of misregistration of the projections on spatial resolution of CT scanners

Marie Foley Kijewski[a)]

Department of Environmental Health Sciences, Harvard School of Public Health, Boston, Massachusetts 02115

Philip F. Judy

Department of Radiology, Harvard Medical School and Brigham and Women's Hospital, Boston, Massachusetts 02115

(Received 20 April 1982; accepted for publication 8 October 1982)

Misregistration of the projections in 360° computed tomographic (CT) scanners has been found to blur the image without generating artifacts. The effects of this error were investigated by analytical methods and by reconstruction of real and simulated data. The point-spread function which results from shifting each projection by a constant distance ϵ consists of a two-dimensional impulse function surrounding a region of negative density. The locus of the impulse function is a circle for parallel-beam geometry and a sixth-order curve for fanbeam geometry. The anisotropy and position dependence of the point-spread function in fanbeam geometry have been characterized. The line-spread function due to the error in parallel-beam geometry consists of two delta functions located at $\pm\epsilon$. In fanbeam geometry, the line-spread function consists of two delta functions separated by approximately 2ϵ, with the locations of the impulses dependent on the position and orientation of the line. This error, combined with other sources of blurring, results in a system edge-response function which contains a flat region at one-half the maximum density.

Key words: computed tomography, image reconstruction, point-spread function, fanbeam geometry, registration error, artifacts

I. INTRODUCTION

Accurate reconstruction of projections measured by computed tomographic (CT) scanners requires correct registration of the projections. Improper specification of the ray which intersects the center of rotation of the scanner will shift each projection by a constant amount (Fig. 1). Shepp *et al.*[1] demonstrated, using parallel-beam geometry, that in 180° scanners this error results in a distinctive pattern of streaks emanating from high-density objects, which they named the tuning fork artifact. They also suggested that scanning over 360° would not eliminate the artifact, although it would reduce its magnitude and alter its characteristics. We have investigated the effects of misregistration of the projections in 360° scanners, in both parallel- and fanbeam geometry, by analysis and by reconstruction of real and simulated data. In analyzing this error, we assumed that the shift of data is constant in all views, and that the projections are sampled along a straight line, i.e., by translation of a source–detector assembly or by a linear array of detectors. We have concluded, based on the results of mathematical analysis, that the only consequence of this error in 360° scanners is a degradation of spatial resolution; contrary to the prediction of Shepp *et al.*,[1] no artifacts[2] are generated. The blurring due to a registration error can be characterized, just as are other component of resolution, by point-spread functions (PSF), line-spread functions (LSF), and edge-response functions (ERF).

Scanners with continuous detectors, in which the position information is determined by electronic means rather than by the physical positions of discrete detector elements, are particularly susceptible to registration errors. One such system is an experimental radioisotope CT scanner[3] which we have used in this work. Because position along its detector, a one-dimensional gamma camera, is determined by electronic delay lines, the position of the central ray varies and must be measured before each scan. CT devices in which image intensifiers serve as detectors, such as the tomographic system described by Kak *et al.*[4] and the Dynamic Spatial Reconstructor,[5] are also susceptible to these errors, as are single-photon emission CT scanners with gamma cameras as detectors.[6]

Two methods of analyzing the effects of misregistration of the projections have been developed. The first method, described in Sec. II, is a derivation of the LSF due to the error in parallel-beam geometry. The results of this analysis prove that the error generates no artifacts. The second method, described in Sec. III, is a means of obtaining a partial description of the PSF of the error by determining the envelope of the shifted and backprojected rays. By this method, the anisotropy and position dependence of the PSF in divergent-beam geometry were characterized.

 0094-2405/83/020169-07$01.20

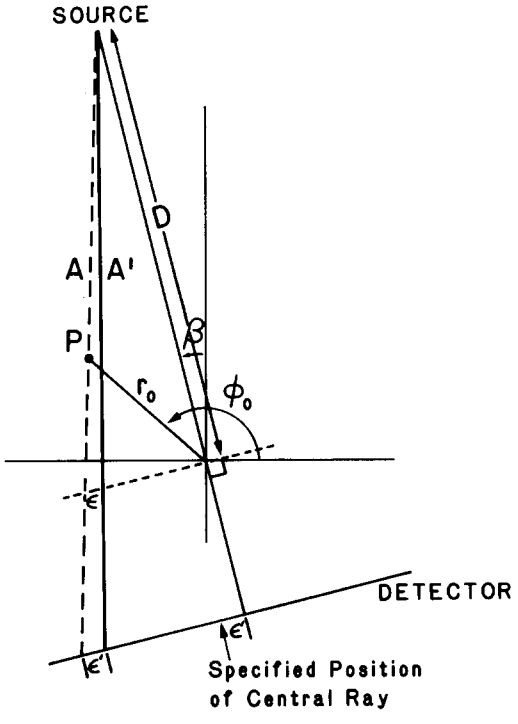

FIG. 1. Illustration of registration error in fanbeam geometry, with source center of rotation distance D. The coordinate system has been defined with the origin at the center of rotation. Ray A has passed through point P, located at (r_0,ϕ_0), during measurement of the view at angle β. An error in the specification of the point at which the central ray intersects the detector has shifted the projection, and the data which should be backprojected along ray A is instead backprojected along ray A'. The equation of the line A' is Eq. (17) in the text.

II. METHOD I: DERIVATION OF LINE-SPREAD FUNCTION IN PARALLEL-BEAM GEOMETRY

In parallel-beam geometry, the rays along which the data within a given projection are measured and backprojected are parallel. As a result, in the limit of continuous angular views, the convolution filter and PSF are stationary and circularly symmetric. In this section, we derive for 360° scanners the LSF resulting from backprojection in parallel-beam geometry of projections which have been shifted by a constant amount ϵ and filtered by

$$H(f)=\begin{cases}|f| \text{ for } |f|<\dfrac{1}{2\tau}\\ 0 \text{ for } |f|>\dfrac{1}{2\tau}\end{cases}, \tag{1}$$

where τ is the sampling distance. The LSF for continuous projections is then obtained by allowing τ to approach zero. In the limit of infinitely fine sampling, all commonly used reconstruction filters are equivalent; therefore, the results of this analysis are independent of the apodization filter.

Because in parallel-beam geometry the PSF $p_\epsilon(r)$ is circularly symmetric, the LSF $l_\epsilon(x)$ is its Abel transform. (The subscript denotes a registration error.) The PSF can be obtained by[7]

$$p_\epsilon(r)=\frac{1}{2\pi}\int_0^{2\pi} h(r\cos\psi-\epsilon)d\psi\,. \tag{2}$$

$h(r)$ is the inverse Fourier transform of $H(f)$:

$$h(r)=\frac{1}{2\tau^2}\operatorname{sinc}\left(\frac{r}{\tau}\right)-\frac{1}{4\tau^2}\operatorname{sinc}^2\left(\frac{r}{2\tau}\right), \tag{3}$$

where

$$\operatorname{sinc}(t)\equiv\sin(\pi t)/(\pi t)\,.$$

Because of the difficulty in evaluating $p_\epsilon(r)$ analytically by Eqs. (2) and (3), an alternative approach was adopted whereby $l_\epsilon(x)$ was obtained without explicitly evaluating $p_\epsilon(r)$. $l_\epsilon(x)$ can be obtained by Fourier transform of the Hankel transform of $p_\epsilon(r)$, since an Abel transform is equivalent to a (zero-order) Hankel transform followed by a one-dimensional Fourier transform. The next step, therefore, is to derive the Hankel transform of $p_\epsilon(r)$.

Convolution and backprojection are linear processes; therefore, the usual order can be reversed. The PSF, $p_\epsilon(r)$, can be expressed as the two-dimensional convolution of the PSF $g_\epsilon(r)$ of simple backprojection of shifted projections with a two-dimensional filter $f(r)$:

$$p_\epsilon(r)=g_\epsilon(r)**f(r)\,, \tag{4}$$

where the double asterisk denotes two-dimensional convolution. By the convolution theorem,[8] the Hankel transform of $p_\epsilon(r)$ equals the product of the Hankel transforms of $g_\epsilon(r)$ and $f(r)$. It is shown in the appendix that

$$g_\epsilon(r)=\frac{[1-\operatorname{rect}(r/2\epsilon)]}{\pi\sqrt{r^2-\epsilon^2}}, \tag{5}$$

where

$$\operatorname{rect}(t)=\begin{matrix}1 \text{ for } |t|<\frac{1}{2}\\ 0 \text{ for } |t|>\frac{1}{2}\end{matrix}. \tag{6}$$

The Hankel transform of $g_\epsilon(r)$ is[9]

$$H[g_\epsilon(r)]=\frac{\cos(2\pi\epsilon\rho)}{\rho}. \tag{7}$$

Since the filter is independent of the registration of the projections, the Hankel transform of $f(r)$ can be found by considering the PSF of correctly registered projections.

The PSF $p(r)$ which results from filtered backprojection of correctly registered projections can be expressed as a two-dimensional convolution of the PSF $g(r)$ of unfiltered backprojection with $f(r)$:

$$p(r)=g(r)**f(r)\,. \tag{8}$$

It has been shown by Barrett and Swindell[10] that

$$p(r)=\frac{J_1(\pi r/\tau)}{2\pi r\tau}, \tag{9}$$

where $J_1(\cdot)$ is a first-order Bessel function of the first kind. It is shown in the appendix that

$$g(r)=\frac{1}{\pi r}. \tag{10}$$

Since[8]

$$H[p(r)]=\frac{1}{\pi}\operatorname{rect}(\tau\rho)\,, \tag{11}$$

and

$$H[g(r)]=\frac{1}{\pi\rho}\,, \tag{12}$$

the Hankel transform of $f(r)$ is

$$H[f(r)] = \frac{H[p(r)]}{H[g(r)]} = \rho \text{ rect } (\tau\rho) . \quad (13)$$

Therefore, the Hankel transform of $p_\epsilon(r)$ is

$$H[p_\epsilon(r)] = H[g_\epsilon(r)]H[f(r)] = \text{rect } (\tau\rho) \cos (2\pi\epsilon\rho) . \quad (14)$$

The LSF $l_\epsilon(x)$ can now be found by Fourier transform of $H[p_\epsilon(r)]$. Using the modulation theorem,[8] we obtain

$$l_\epsilon(x) = \frac{1}{2\tau} \text{sinc} \left(\frac{x-\epsilon}{\tau}\right) + \frac{1}{2\tau} \text{sinc} \left(\frac{x+\epsilon}{\tau}\right), \quad (15)$$

which becomes, as $\tau \to 0$,

$$l_\epsilon(x) = \tfrac{1}{2}\delta(x-\epsilon) + \tfrac{1}{2}\delta(x+\epsilon) . \quad (16)$$

Thus, the LSF is a pair of delta functions located at $x = \pm\epsilon$. We can deduce that its inverse Abel transform, the PSF, consists of a two-dimensional impulse function of radius ϵ, surrounding a region of negative density. This implies that a registration error which is constant in all projections does not affect the image at distances from the object greater than its magnitude and, therefore, generates no artifacts.

III. METHOD II: ENVELOPE ANALYSIS

The image formed by simple (unfiltered) backprojection of a number of properly registered projections of a point density is a set of lines which intersect at a point [Fig. 2(a)]. Convolution of the projections with a suitable filter before backprojection eliminates these lines, and in the limit of continuous projections and continuous angular views, the image is a point. In Fig. 2(b), the image resulting from unfiltered backprojection of a number of improperly registered projections of a point density is shown. As the number of views increases, a smooth curve is formed at the intersections of the lines. The results of the last section imply that in parallel-beam geometry, convolution of the projections before backprojection with the same filter will eliminate the lines, resulting (in the continuous case) in zero reconstructed density in the area outside the curve. We will assume for the purposes of this analysis that this is also true in fanbeam geometry. The filter will also contribute negative densities to the region inside the curve. The PSF due to a registration error, therefore, consists of a region of negative density surrounded by a ridge, or two-dimensional impulse function, which lies along the curve formed by the intersections of the backprojected rays.

In this section, we describe the method used to find the locus of this impulse function, which forms the boundary of the PSF. Although this method does not provide a complete description of the PSF, since it gives no information on the interior, it does provide information on the spatial extent of the PSF as a function of position in the reconstruction plane, geometry of the scanner, and magnitude of the error. Combining the results of this section with those of the previous section gives the LSF due to the error for fanbeam geometry.

The set of lines formed by continuous variation of a parameter is known as a family of lines, and the curve to which all members of the family are tangent, as the envelope. Mathematical methods of deriving an expression for the envelope

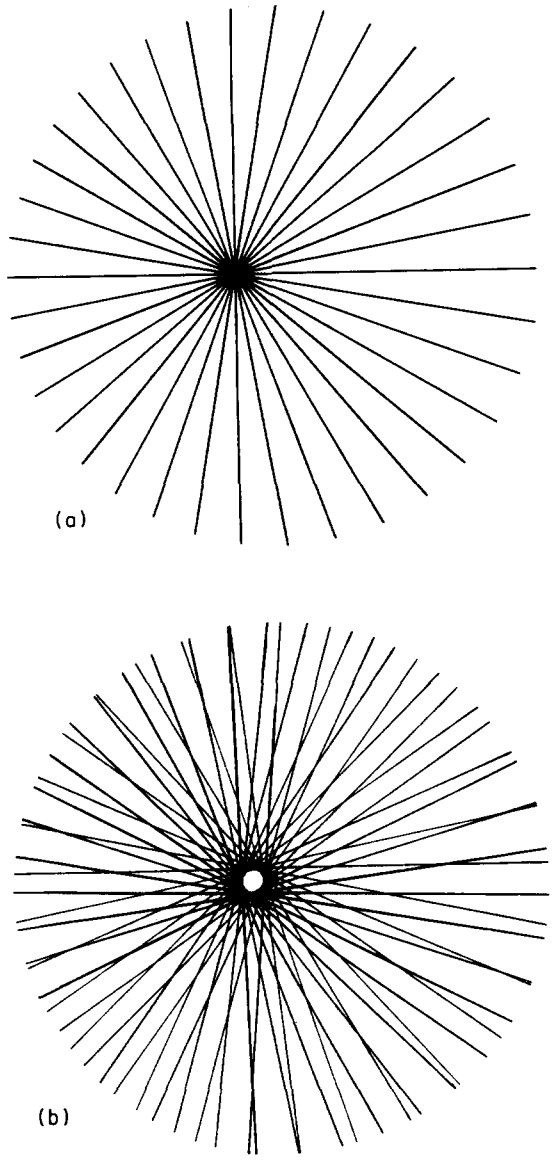

FIG. 2. (a) Image formed by simple backprojection of 36 properly registered views of a point density. (b) Image formed by simple backprojection of 72 misregistered views of a point density.

from the parametric equation of the lines have been developed.[11] The envelope of a family of lines whose equation is a polynomial in the parameter can be found by setting the discriminant of the equation with respect to the parameter equal to zero.

Each view contributes to the image a line whose equation is

$$\frac{r\cos(\beta-\phi)}{1+(r/D)\sin(\beta-\phi)} - \frac{r_0\cos(\beta-\phi_0)}{1+(r_0/D)\sin(\beta-\phi_0)} - \epsilon = 0 . \quad (17)$$

The variables have been defined in Fig. 1. The continuously varying parameter is the view angle β. Substituting $\beta = 2 \arctan(t)$ into Eq. (17) gives a quartic equation in the new parameter t:

$$t^4 + bt^3 + ct^2 + dt + e = 0 , \quad (18)$$

where the coefficients b, c, d, and e are functions of r_0, ϕ_0, r, ϕ,

D, and ϵ. The discriminant of a quartic equation is[12]

$$f(r,\phi) = 4[bd - 4e - (1/3)c^2]^3 + 27[-b^2e + (1/3)bcd + (8/3)ce - d^2 - (2/27)c^3]^2 . \quad (19)$$

Therefore, the envelope is the curve S defined by $f(r,\phi) = 0$.

For the special case of parallel-beam geometry ($D \to \infty$), $f(r,\phi) = 0$ is the equation of a circle of radius ϵ centered at (r_0,ϕ_0). For fanbeam geometry, the expressions for b, c, d, and e were substituted into Eq. (19) using MACSYMA,[13] a computer program that is capable of symbolic algebraic manipulation. The result is an irreducible sixth-order expression of more than 1000 terms. Therefore, the points belonging to the envelope [the roots of Eq. (19)] were determined numerically.[14] In fanbeam geometry, the PSF due to a registration error is nonisotropic and dependent on radius. The PSF at points located at equal radii but different angular positions differ only by a rotation about the origin. In this respect, the blurring due to a registration error resembles that due to the finite source–detector aperture, which was described by Verly and Bracewell.[15]

The LSF can be obtained from the PSF by integrating over one rectangular coordinate. The contribution to the LSF of the registration error from the impulse function lying along the envelope S is [Fig. 3(a)]

$$l'_\epsilon(x) = \int_{-\infty}^{\infty} \delta_2(S)dy , \quad (20)$$

where $\delta_2(\cdot)$ is a two-dimensional Dirac delta function.[16] If the complete PSF were integrated over one variable, the negative densities in the interior would tend to cancel the positive densities along the boundary, reducing the central portion of $l'_\epsilon(x)$. In Sec. II, we showed that in parallel-beam geometry this cancellation is exact, and the LSF consists of a pair of delta functions; because the PSF is stationary and isotropic, the LSF is independent of position and orientation. In fanbeam geometry, assuming that this cancellation is also exact, the LSF [Fig. 3(b)] is a pair of delta functions, separated by approximately 2ϵ, with their locations dependent on radius and orientation of the line, as summarized in Fig. 4. The parameters which we have used to characterize the position dependence of the blurring are the widths of the LSF on either side of the line, $W1$ and $W2$ (Fig. 3).

For parallel-beam geometry, the full width of the LSF (or ERF) is twice the magnitude of the registration error, and the LSF is symmetric. $W1$ and $W2$ each equal ϵ, independent of position and orientation. For fanbeam geometry, the full width of the LSF is approximately twice the magnitude of the error, but the distribution of the width on either side of the line depends on distance from the origin and orientation (Fig. 4). Although the total width of the LSF is (almost) independent of radius, the degree of asymmetry increases with distance from the origin.

This analysis implies that combining a registration error with other components of resolution will increase the width of the ERF, and that the composite ERF will contain a flat region of one-half the maximum density. For fanbeam geometry, the distribution of the increase in width between the sides of the edge will depend on the location and orientation of the edge.

IV. EXPERIMENTS

A. Measurements

Projection data were measured on the experimental radioisotope CT scanner. The source is ^{137}Cs, which emits a single 662-keV photon. The distance from the source to the center of rotation is 90 cm. The detector, which has been described by Maddox *et al.*,[3] is a one-dimensional gamma camera, a $40 \times 5 \times 1.25$ cm^3 NaI crystal coupled to an array of photomultiplier tubes. The detector output is transmitted to a multichannel analyzer, the channels of which correspond to position along the crystal.

An 11.5×5.0 cm^2 rectangular Plexiglas phantom was scanned in air on this device. Images were reconstructed

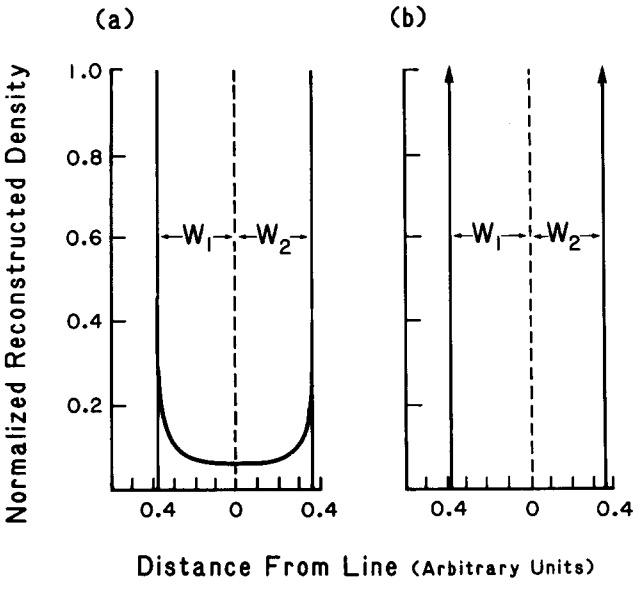

FIG. 3. (a) Contribution to LSF of registration error from impulse function which bounds PSF. (b) Total LSF of registration error. Parameters of resolution $W1$ and $W2$ are widths of LSF on either side of the line.

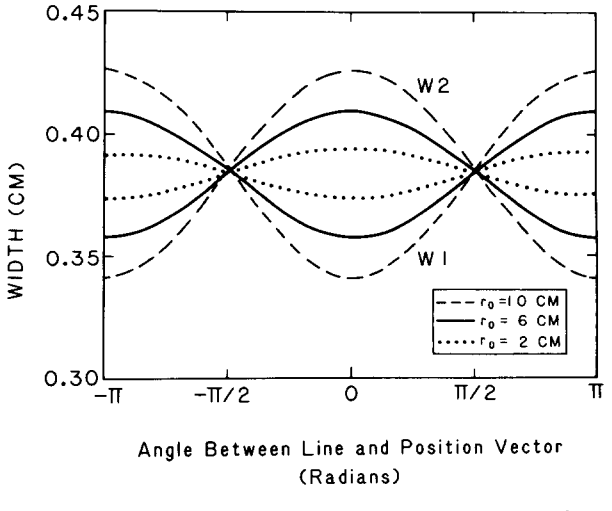

FIG. 4. Dependence of $W1$ and $W2$ on radius and orientation, fanbeam geometry, $\epsilon = 0.373$ cm, $D = 90$ cm.

from 360 projections at 1° increments by the convolution-backprojection method, as modified for fanbeam geometry by Herman *et al.*,[17] with a Hanning filter[18] substituted for the ramp filter. Each projection consisted of 270 data points; the sampling distance, referred to a line intersecting the center of rotation, was 0.0766 cm.

Images of the phantom were reconstructed from correctly registered projections [Fig. 5(a)] and from projections which had been shifted by five channels (0.373 cm) [Fig. 5(b)], an arbitrary error chosen to clearly illustrate the effects of shifting the projections. The edges are blurred, and the density in the blurred region is one-half the maximum.

B. Simulations

Simulations were performed to eliminate from the image the effects of focal spot size, detector resolution, and noise. Images were reconstructed as described above from calculated projections of a rectangular object. Both parallel- and fanbeam geometries were simulated.

In Figs. 5(c) and 5(d) are shown images reconstructed from simulated profiles in the geometry of the radioisotope scanner, with and without a registration error. The characteristic blurred area at one-half the maximum density is evident. In Fig. 5(e) is shown an image analogous to that in Fig. 5(d), but with the distance from the source to the center of rotation reduced from 90 to 30 cm in order to increase the anisotropy of the PSF. The blurring due to the error is again evident; in addition, because of the anisotropy of the PSF, the width of the blurred region varies along the edges. The anisotropy of the PSF in fanbeam geometry is more clearly demonstrated in a difference image between reconstructions with registration errors of equal magnitude but opposite sign [Fig. 5(f)]. In parallel-beam geometry, such an image would be zero everywhere. The streaks which emanate from the edges in Fig. 5(f) are due to aliasing and not to the registration error. Similar streaks can be seen in Fig. 5(c), which was reconstructed from correctly registered projections. The image shown in Fig. 5(f) is displayed on a different gray scale than the others, making the streaks more prominent.

ERF were obtained from simulated data by calculating reconstructed density at 0.01-cm intervals along a line perpendicular to an edge and intersecting it at the point of interest. The predicted flat region at one-half the maximum density is evident in the ERF for misregistered projections (Fig. 6).

We have used unsharpness,[19] a single-parameter measure of blurring, to characterize resolution. It is defined as the distance between the points at which the values of the normalized ERF are 0.165 and 0.835. For Gaussian distributions, the unsharpness is equal to twice the standard deviation of the LSF. Here we have separated the unsharpness into the distance between the points at which the values of the ERF are 0.165 and 0.5 ($U1$) and the distance between the points at which they are 0.5 and 0.835 ($U2$).

ERF were calculated for a number of orientations at various points in the reconstruction plane. The measured ERF were independent of position and orientation for parallel-beam geometry, and dependent on radius and orientation for

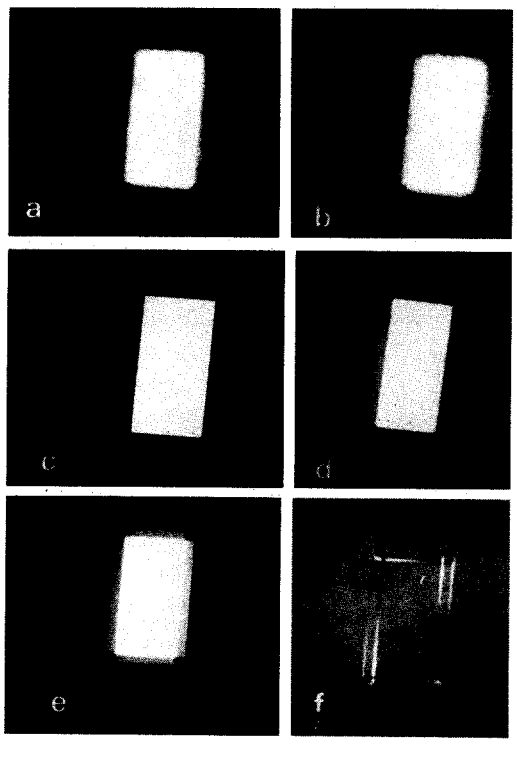

FIG. 5. (a) Image of rectangular phantom, radioisotope scanner, fanbeam geometry, $D = 90$ cm, $\epsilon = 0$. (b) Image of rectangular phantom, radioisotope scanner, fanbeam geometry, $D = 90$ cm, $\epsilon = 0.373$ cm. (c) Image of simulated rectangular phantom, fanbeam geometry, $D = 90$ cm, $\epsilon = 0$. (d) Image of simulated rectangular phantom, fanbeam geometry, $D = 90$ cm, $\epsilon = 0.373$ cm. (e) Image of simulated rectangular phantom, fanbeam geometry, $D = 30$ cm, $\epsilon = 0.373$ cm. (f) Difference between images of simulated rectangular phantom, fanbeam geometry, $D = 30$ cm, $\epsilon = \pm 0.373$ cm.

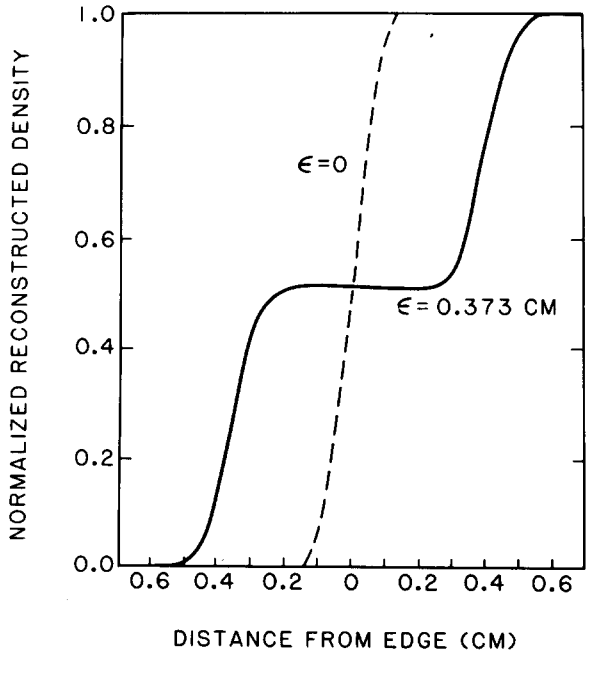

FIG. 6. ERF calculated from simulated data, fanbeam geometry, $r_0 = 8.0$ cm, $D = 90$ cm. Dashed line represents ERF for correctly registered projections, solid line, ERF for projections shifted by 0.373 cm.

fanbeam geometry. When $U1$ and $U2$ are compared with $W1$ and $W2$ of the LSF calculated in Sec. II, it is apparent that the predicted position and orientation dependence of the effects of the registration error in fanbeam geometry are verified (Fig. 7). $U1$ and $U2$ are greater than $W1$ and $W2$ because they include the blurring due to the reconstruction filter.

V. DISCUSSION

Shepp *et al.*[1] showed that in 180° scanners, a registration error as small as 0.05 mm results in a clearly visible artifact. We have shown here that in 360° scanners, contrary to their prediction,[20] a registration error results in no artifacts. The width of the LSF due to the error is approximately twice the magnitude of the error; in a high-resolution CT scanner, registration errors of less than 1 mm can result in blurring which is significant compared to that due to other sources. Because misregistration of the projections results in a subtle deterioration of image quality rather than in a clearly visible artifact, the presence of this error may not be recognized. A system ERF with a flat region at 50% of maximum density is an indication of this source of blurring.

The form of the LSF due to the registration error provides an intuitive explanation of the tenet[21,22] that, for continuous projections and views, the LSF of the image is the aperture function. If a symmetric aperture function is decomposed into a series of appropriately scaled and shifted delta functions, with each shift considered a "registration error," summation of the resultant "registration error" LSF will reproduce the aperture function.

The effects of a registration error may explain some previously reported observations. Moran and Perman[23] measured abrupt variations in LSF and, consequently, significant high-frequency components in the modulation transfer functions (MTF). Errors in registration generate discontinuous LSF; these may be the source of the high-frequency components of the MTF. This does not explain the anomalous low-frequency noise power component which Moran and Perman discussed, because the noise power spectrum is not affected by misregistration or by any other geometric change in the physical aperture.

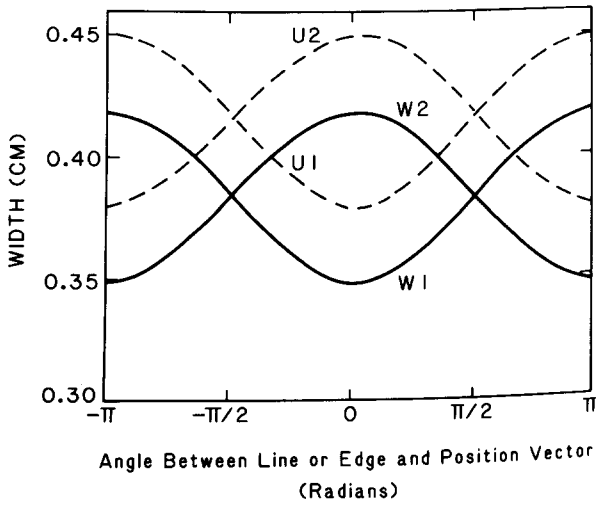

FIG. 7. Dependence of $W1$, $W2$, $U1$, $U2$ on orientation, fanbeam geometry, $r_0 = 8.0$ cm, $\epsilon = 0.373$ cm, $D = 90$ cm.

ACKNOWLEDGMENTS

We are grateful to the Joint Center for Radiation Therapy and Department of Radiation Therapy, Harvard Medical School, for the use of the radioisotope scanner and computer facilities. We thank Bruce Lulu for many valuable discussions and Ellen Hildreth for assistance with MACSYMA. We thank P. R. Moran and Norbert Pelc for critical reading of the manuscript and valuable suggestions. This work was supported by NIH Grant Number S07 RR 05526, NCI Grant Number 5T32 CA 09088, and PHS Grant Number GM 18674.

APPENDIX

Here the PSF which result from unfiltered backprojection of properly and of improperly registered projections are calculated. For properly registered projections, the PSF $g(r)$ is

$$g(r) = \frac{1}{2\pi}\int_0^{2\pi} \delta(r\cos\psi)d\psi\,, \tag{A1}$$

where $\delta(\cdot)$ is a one-dimensional Dirac delta function.[8] Because the Fourier transform of $\delta(t)$ is 1, we have

$$g(r) = \frac{1}{2\pi}\int_0^{2\pi}\int_{-\infty}^{\infty} \exp[i2\pi f r\cos\psi]\,df\,d\psi\,. \tag{A2}$$

Reversing the order of integration, and using the identity[9]

$$J_0(t) = \frac{1}{2\pi}\int_0^{2\pi} \exp[it\cos\psi]d\psi\,, \tag{A3}$$

we obtain the well-known[24] result

$$g(r) = \int_{-\infty}^{\infty} J_0(2\pi f r)df = \frac{1}{\pi r}\,. \tag{A4}$$

For projections which have been shifted by ϵ, the PSF $g_\epsilon(r)$ is

$$\begin{aligned} g_\epsilon(r) &= \frac{1}{2\pi}\int_0^{2\pi} \delta(r\cos\psi - \epsilon)d\psi \\ &= \frac{1}{2\pi}\int_{-\infty}^{\infty} \exp[-i2\pi f\epsilon] \\ &\quad\times\int_0^{2\pi} \exp[i2\rho f r\cos\psi]d\psi\,df \\ &= \int_{-\infty}^{\infty} \cos(2\pi f\epsilon)J_0(2\pi r f)df\,. \end{aligned} \tag{A5}$$

Evaluating the integral,[25] we obtain

$$g_\epsilon(r) = \frac{[1 - \text{rect}\,(r/2\epsilon)]}{\pi\sqrt{r^2 - \epsilon^2}}\,. \tag{A6}$$

[a] Mailing address: Division of Physics and Engineering, Room 128, 44 Binney Street, Boston, Massachusetts 02115.

[1] L. A. Shepp, S. K. Hilal, and R. A. Schulz, Comput. Graphic Image Proc. **10**, 246 (1979).

[2]We define artifacts as errors in the image which extend into portions of the image well beyond the immediate vicinity of the object causing them.
[3]B. J. Maddox, J. M. Galvin, K. R. Kase, J. C. Leong, and B. E. Bjarngard, Nucl. Instrum. Methods. **190**, 377 (1981).
[4]A. C. Kak, C. V. Jakowatz, N. A. Baily, and R. A. Keller, IEEE Trans. Biomed. Eng. **BME-24**, 157 (1977).
[5]R. A. Robb, E. L. Ritman, B. K. Gilbert, J. H. Kinsey, L. D. Harris, and E. H. Wood, IEEE Trans. Nucl. Sci. **NS-26**, 2713 (1979).
[6]T. F. Budinger, S. E. Derenzo, G. T. Gullberg, W. L. Greenberg, and R. H. Huesman, J. Comput. Assist. Tomogr. **1**, 131 (1977).
[7]E. Tanaka and T. A. Iinuma, Phys. Med. Biol. **20**, 789 (1975).
[8]R. N. Bracewell, *The Fourier Transform and Its Applications* (McGraw-Hill, New York, 1978).
[9]J. D. Gaskill, *Linear Systems, Fourier Transforms, and Optics* (Wiley, New York, 1978).
[10]H. H. Barrett and W. Swindell, Proc. IEEE **65**, 89 (1977).
[11]J. Edwards, *Elementary Treatise on the Differential Calculus* (MacMillan, London, 1892).
[12]L. E. Dickson, *Elementary Theory of Equations* (Wiley, New York, 1914).
[13]MACSYMA was developed by the Mathlab Group, Laboratory for Computer Science, Massachusetts Institute of Technology. The work of the Mathlab Group is supported, in part, by the United States Energy Research and Development Administration under Contract Number E(11-1)-3070 and by the National Aeronautics and Space Administration under Grant Number NSG 1323.
[14]For a given ϕ, the value of r for which $f(r,\phi)$ was zero was found by calculating $f(r,\phi)$ for a series of values of r. For each ϕ, the sign of $f(r,\phi)$ changed once over a large range of r, and the root could be determined to any desired accuracy by evaluating $f(r,\phi)$ at smaller increments of r.
[15]J. G. Verly and R. N. Bracewell, J. Comput. Assist. Tomogr. **3**, 662 (1979).
[16]Equation (20) was evaluated using the definitions of $\delta_2(S)$ and $\delta_2[f(x,y)]$ from p. 94 of Ref. 9 and the sifting property of the delta function:

$$l'_\epsilon(x) = \frac{\sqrt{\frac{\partial}{\partial x}[f(x,y_n)]^2 + \frac{\partial}{\partial y}[f(x,y_n)]^2}}{\left|\frac{\partial}{\partial y}[f(x,y_n)]\right|}.$$

To calculate $l'_\epsilon(x)$ for a line located at (r_0,ϕ_0) and oriented at an arbitrary angle θ to ϕ_0, the coordinate system is translated to (r_0,ϕ_0) and rotated through $\alpha = \phi_0 + \pi/2 - \theta$, and $l'_\epsilon(x)$ re-expressed in terms of the transformed coordinates. Expressions for $(\partial/\partial x')[f(x',y')]$ and $(\partial/\partial y')[f(x',y')]$ were obtained by differentiation of Eq. (19) and coordinate transformation. The values of the partial derivatives at x',y' were calculated using a digital computer.
[17]G. T. Herman, A. V. Lakshminarayanan, and A. Naparstek, Comput. Biol. Med. **6**, 259 (1976).
[18]D. A. Chesler and S. J. Riederer, Phys. Med. Biol. **20**, 632 (1975).
[19]R. E. Shuping and P. F. Judy, Med. Phys. **5**, 491 (1978).
[20]The fact that a registration error causes no artifacts in 360° scanners can also be shown using the approach of Shepp *et al.* (Ref. 1). Converting Eq. (6) of Ref. 1 to polar coordinates r,ϕ and changing the upper limit of integration to 2π gives, for $r > b + \delta$,

$$\frac{1}{D}f^*(r,\phi) = 1 - \frac{1}{\pi}\left\{\int_\xi^{1-u} \frac{t\,dt}{\sqrt{(t^2-\xi^2)[1-(t+u)^2]}} + \int_\xi^{1+u} \frac{t\,dt}{\sqrt{(t^2-\xi^2)[1-(t-u)^2]}}\right\}.$$

The integrals can be re-expressed in terms of complete elliptic integrals using formula 3.1487 of Ref. 25:

$$\frac{1}{D}f^*(r,\phi) = 1 - \frac{1}{\pi}\frac{4}{\sqrt{(1+\xi)^2-u^2}}\{\Pi(n,k) + \Pi(k^2/n,k) - K(k)\}.$$

$$n \equiv \frac{(\xi-1)+u}{(\xi+1)+u}; \quad k^2 \equiv \frac{(1-\xi)^2-u^2}{(1+\xi)^2-u^2}.$$

Formula 117.02 of Ref. 26 states, for $n < 0$

$$\Pi(n,k) + \Pi(k^2/n,k) = K(k) + (\pi/2)\sqrt{\frac{n}{(1-n)(n-k^2)}}.$$

Therefore, for points in the image at distances from the object greater than the magnitude of the registration error,

$$\frac{1}{D}f^*(r,\phi) = 0.$$

[21]L. A. Shepp and J. B. Kruskal, Am. Math. Mon. **85**, 420 (1978).
[22]P. M. Joseph, R. D. Spital, and C. D. Stockham, Comput. Tomogr. **4**, 189 (1980).
[23]P. R. Moran and W. H. Perman (personal communication).
[24]R. A. Brooks and G. DiChiro, Phys. Med. Biol. **21**, 689 (1976).
[25]I. S. Gradshteyn and I. M. Ryzhik, *Table of Integrals, Series, and Products* (Academic, New York, 1980).
[26]P. F. Byrd and M. D. Friedman, *Handbook of Elliptic Integrals for Engineers and Physicists* (Springer, Berlin, 1954).